LAWRENCE
LIVERMORE
NATIONAL
LABORATORY

LLNL-PROC-401717

Nansecond time resolved investigations using the in situ of Dynamic Transmission Electron Microscope (DTEM)

T. LaGrange, G. H. Campbell, B. W. Reed, M. L. Taheri, J. B. Pesavento, J. S. Kim, N. D. Browning

February 27, 2008

Frontiers in Electron Microscopy and Materials Science
Rohnert Park, CA, United States
September 23, 2007 through September 28, 2007

Disclaimer

This document was prepared as an account of work sponsored by an agency of the United States government. Neither the United States government nor Lawrence Livermore National Security, LLC, nor any of their employees makes any warranty, expressed or implied, or assumes any legal liability or responsibility for the accuracy, completeness, or usefulness of any information, apparatus, product, or process disclosed, or represents that its use would not infringe privately owned rights. Reference herein to any specific commercial product, process, or service by trade name, trademark, manufacturer, or otherwise does not necessarily constitute or imply its endorsement, recommendation, or favoring by the United States government or Lawrence Livermore National Security, LLC. The views and opinions of authors expressed herein do not necessarily state or reflect those of the United States government or Lawrence Livermore National Security, LLC, and shall not be used for advertising or product endorsement purposes.

Nanosecond time resolved investigations using the *in situ* of Dynamic Transmission Electron Microscope (DTEM)

Thomas. LaGrange*
Lawrence Livermore National Laboratory, 7000 East Avenue, Livermore, California 94550

Geoffrey H. Campbell, B. W. Reed, Mitra Taheri, J. Bradley Pesavento
Lawrence Livermore National Laboratory, 7000 East Avenue, Livermore, California 94550

Judy S. Kim and Nigel D. Browning
Lawrence Livermore National Laboratory, 7000 East Avenue, Livermore, California 94550
And Department of Chemical Engineering and Materials Science, University of California, One Shields Avenue, Davis, California 95616

Abstract

Most biological processes, chemical reactions and materials dynamics occur at rates much faster than can be captured with standard video rate acquisition methods in transmission electron microscopes (TEM). Thus, there is a need to increase the temporal resolution in order to capture and understand salient features of these rapid materials processes. This paper details the development of a high time resolution dynamic transmission electron microscope (DTEM) that captures dynamics in materials with nanosecond time resolution. The current DTEM performance, having a spatial resolution <10 nm for single-shot imaging using 15 ns electron pulses, will be discussed in the context of experimental investigations in solid state reactions of NiAl reactive multilayer films, the study of martensitic transformations in nanocrystalline Ti and the catalytic growth of Si nanowires. In addition, this paper will address the technical issues involved with high current, electron pulse operation and the near term improvements to the electron optics, which greatly improve the signal and spatial resolutions, and to the laser system, which allow tailored specimen and photocathode drive conditions.

Keywords: Ultrafast electron diffraction, time resolved electron microscopy, catalysis, martensitic phase transformations

* corresponding author, email: lagrange@llnl.gov

1. Introduction

There have been many advances in the past decade to improve the spatial resolution of transmission electron microscopes [1, 2]. However, there have been limited efforts to improve the temporal resolution of the *in situ* transmission electron microscopy beyond nominal video acquisition rates. Many processes in chemistry, biology and materials science proceed at rates much faster than the 33 ms frame speed of standard video [3, 4]. In order to capture the transient events of these processes, the temporal resolution must be extended beyond this video rate limitation. The temporal resolution can be improved by controlling the electron emission, such that it is correlated in time with the transient process being studied, similar to the approach taken in ultrafast electron diffraction and X-ray pump-probe techniques [5-8].

In the pump-probe approach, a transient state is first driven in the material, for example, by an initiating laser pulse, and then examined by a later analytical pulse of electrons at a correlated time with the initiating pulse. To study irreversible processes, the analytical pulse must contain a sufficient number of electrons to acquire a snapshot of the transient events in that process (single-shot approach [9]). Alternatively, if the process is reversible, an image or diffraction pattern can be formed by the integration of multiple pump and probe cycles (stroboscopic approach). The caveats to the single-shot approach are that it requires a high brightness source ($>10^9$ A cm^{-2} steradian^{-1}) and that electron-electron interactions in high current electron pulses will limit spatial resolution. In addition, modern TEMs are not designed for high current operation necessary for the single-shot technique, and thus, the instrument must be modified and optimized to accommodate high current pulsed electron probes, making it a much more technically challenging approach. Yet despite its difficulties, the single-shot approach is worth pursuing because it dramatically widens the range of phenomena that may be studied, since

most processes of interest in materials science are irreversible. An ongoing effort at Lawrence Livermore National Laboratory (LLNL) has focused on the single-shot approach, developing a dynamic transmission electron microscope (DTEM) with this capability [4, 9-11].

In this article, we discuss the design and construction of the DTEM for single-shot operation. In its current state, the DTEM achieves a spatial resolution better than 10 nm using 15ns electron pulses. The spatial resolution, at present, is dose limited due to the poor coupling between the gun and condenser lens system and the limited brightness of the source. Recent improvements to the electron optics will be discussed that have both increased current and preserved electron source brightness, followed by a description of near-term improvements to the laser systems and electron optics that will enable the acquisition of multi-frame movies. The latter part of this paper will discuss how we have used the current capabilities of the DTEM to study the transient phase evolution of solid state reactions that occur in NiAl reactive multilayer films, the martensitic nucleation behavior and α to β transformation rates in nanocrystalline Ti, and the catalytic growth of Si nanowires.

2. Current state of art of LLNL DTEM

The DTEM is built on the JEOL 2000FX microscope platform, see Figure 1. The electron optical column has been modified to provide laser access to the photocathode and specimen. A brass drift section has been added between the gun alignment coils and condenser optic that contains a 1" laser port and 45° Mo mirror, which directs an on-axis 211 nm laser pulse to 825μm Ta disk photocathode[1]. The 10ns UV laser pulse photoexcites a ~15ns FWHM electron pulse from the cathode. This pulse is accelerated through the electron gun and passes through a

[1] The Ta disk photocathode can also be used as a thermionic source in nominal TEM operational mode.

hole in the Mo[2] laser mirror into electron optics of the TEM column. The electron pulse is aligned and illuminates specimens as in standard TEM operation, and thus all imaging modes can be utilized, e.g., brightfield, darkfield, selected area electron diffraction.

To better couple the photoemitted electron pulse into the condenser electron optics, a weak lens has been installed above the Mo laser mirror and drift section. The lens provides increased current by focusing the spatially broad pulsed electron beam through the hole in the laser mirror. In prior configurations without the coupling lens, it was found that the mirror was the limiting aperture and reduced the electron current by a factor of 20. The coupling lens combined with appropriate condenser lens settings and imaging conditions preserves the brightness of the photoelectron gun and improves beam quality by reducing the aberrations that can result from a spatially broad electron pulsed and high-angle, off axis electrons. More details on the coupling lens design will be given in the following sections.

Time-resolved experiments in the DTEM are conducted by first initiating a transient state in the sample and then taking a snapshot of the transient process with the 15 ns electron pulse at some specified time delay after the initiation pulse. In most DTEM experiments, the transient process is initiated with a second laser pulse, which enters the TEM column through a modified, high-angle X-ray port. For nanosecond time scale experiments, Neodymium doped YAG lasers with pulse duration from 3 to 25 ns are used that can produce fluences up to 1500 J cm^{-2} on the specimen. The amount of absorbed laser light is dependent on the wavelength, and specimen absorption characteristic can vary. For example, metals have broadband absorption and thus can absorb some amount of light at all wavelengths, while certain semiconductors only absorb sufficient amounts of laser energy in the UV range. In order to produce the desired experimental

[2] Solid molybdenum mirrors have a high reflectivity (>60%) in the UV range, and molybdenum can be easily polished to produce high quality, uniform surfaces (low wavefront distortion) needed for laser applications.

conditions in a variety of specimens, the fundamental wavelength (1064 nm) of these lasers can be frequency converted using non-linear harmonic generation crystals, e.g., doubled (532 nm) or tripled (355 nm).

In a typical DTEM experiment, the instrument and specimen are first aligned in standard, thermionic mode, and then the alignment is optimized further in pulsed mode. Since DTEM pump-probe experiments usually permanently alter the sample, the sample is moved to a new location between shots. The evolution of an irreversible materials process is studied through a series of pump-probe experiments with different time delays. Since the delays used in the DTEM can be microseconds, it is impractical to delay the pulses using an optical delay leg. Instead, time delays are set in the DTEM by electronic triggering, with the synchronization the two laser systems achieved using active diagnostics in the beamline, e.g. photodiodes placed at equivalent distances as the photocathode and specimen, to precisely define the pulse arrival times. Using this method, the pump and probe pulses can be precisely timed within ~1 ns.

2.1 Current Performance of the DTEM

In its current configuration, the DTEM can acquire images with better than 10nm spatial resolution with 15ns electron pulses. An example of the current spatial resolution and image capabilities is given in Figure 2 which shows a cross-sectional view of gold (dark layers) and carbon (light contrast layers) multilayer foil. The individual layer thicknesses are less than 10 nm, and the layers are clearly resolved in the single shot image (Figure 2b). To better illustrate the resolution limits in the single-shot image, the pixel intensity across the multilayer was measured and plotted (see Figure 2). The intensity from 9 nm thick layers is clearly visible above the background, indicating that the resolution is at least 9 nm, if not better.

A critical advancement of LLNL DTEM over prior instruments developed by the Bostanjoglo group [12] is the ability to capture dynamical contrast images. The unique electron source and lens system of the LLNL DTEM allows higher electron beam current and coherence, enabling the use of objective apertures to obtain brightfield and darkfield images of defects such as grain boundaries, dislocations and stacking faults. Figure 3 shows an example of a single-shot, 15-nanosecond exposure 6061 Al sample containing fine precipitates; the dynamical contrast from bend contours is clearly evident. There very little difference between the CW and pulsed image at low magnification with exceptions that the bend contours are slightly wider. The ability to capture dynamical contrast images is an important step in the DTEM's technological development, since these defects play an important role in the mechanical properties of materials, and capturing their dynamics under a transient thermal or mechanical load can provide a better understanding of how the mechanical behavior of the material evolves.

3. Redesigning Electron Optics for Single-shot DTEM

The standard electron optics of modern TEMs are designed to operate with electron beam currents <100 nA. In standard TEM, the electrons generated at the source (several μAs of current for a thermionic source) are blocked by apertures to increase beam coherence and spatial resolution, and often much less than 1% of the generated electrons reach the sample (Figure 4a). This is a practical tradeoff in conventional TEM, since there is sufficient dose in a one second exposure to acquire high quality images using a nanoampere electron beam. However, single-shot operation in the DTEM does not have this luxury. The number of electrons per pulse (10^8-10^9) and signal are low, requiring the use of large apertures and to make a tradeoff between beam coherence and signal. This compromise is necessitated by the limited source brightness, where the required current density at the sample is strictly dictated by temporal resolution and signal-to-

noise ratio requirements (Rose criterion) [13]. The inevitable conclusion is that some sacrifice of spatial coherence is required, which means that the DTEM's condenser system has to be able to handle much wider (or, more precisely, higher-emittance) beams than does a CW TEM. In effect, high-coherence modes such as phase contrast atomic resolution imaging will be extremely challenging on the nanosecond scale, but other modes with less stringent coherence requirements (e.g. mass-thickness and diffraction contrast imaging) are possible, as shown in section 3 and the following sections. While some gains can be made by removing fixed apertures and weakening the C1 lens (Figure 4b), this can still leave well over 90% of the electrons unused, especially when C1 aberrations are considered. This is far from optimal, since the estimated spatial resolution limit due to spatial incoherence (~1 nm) is still far better than the resolution limit due to signal-to-noise ratio (>10 nm).

To solve this problem, a very weak, very large-bore lens (dubbed the C0 lens, since it precedes C1) is being introduced below the accelerator, followed by a long (~20 cm) drift space to allow the beam to reconverge (Figure 4c). The geometry allows a 3 mm diameter portion of the beam to be focused through the 1 mm diameter hole in the mirror and into the center of the C1 lens without introducing excessive aberrations. Simulations of the modified condenser lens system show that the thermal emittance (e.g., the spatial incoherence deriving from the finite source brightness) dominates the effects of condenser lens aberrations when the DTEM is operated in this mode. In other words, the coupling is essentially as good as it can get; even with the large apertures in use, the aberration-induced emittance growth from source to sample is negligible. These simulations coupled with the measured characteristics of the beam at the exit of the accelerator predict that more than 10^9 electrons should be available in a 15 ns pulse at the specimen. This is a 20-fold improvement in beam current compared to the DTEM without the

C0 lens. At this point the system will be limited by the source rather than by the lens and aperture designs, and the signal levels and coherence can be optimized against each other across the entire gamut of foreseeable experiments.

4. Near-Term Instrument Developments

4.1 Arbitrary Waveform Generation Laser System

For most Q-switched, pulsed laser systems, the resonator cavity, lasing medium, and excitation source determine the pulse duration and repetition rate, and thus, these systems have a fixed pulse width, spatial mode and repetition rate. Since the cathode laser pulse and electron pulse duration are similar, the time resolution is fixed by the type of cathode laser system used. Since not all experiments require nanosecond time resolution, a compromise can be made between the temporal and spatial resolutions[3]. For instance, microsecond time resolution is sufficient for some catalytic reactions and dislocation dynamic studies, and these studies can benefit from the added electron dose and increased spatial resolution. To increase flexibility in laser systems and to tailor the laser parameter for a given experiments, we are designing and constructing an arbitrary waveform generation laser (AWG) which can temporally shape laser pulse, thus allowing to easily change the pulse duration.

The AWG is composed of a waveform generator that drives a fiber based electro-optical modulator and temporally shapes a continuous wave fiber laser seed pulse. The modulated waveforms are then amplified, frequency converted and delivered to the DTEM at appropriate energy for use a cathode and specimen drives. The AWG cathode drive laser allows for continuously variable and controlled electron pulse duration from 20 μs down to 10 ns. The AWG sample drive laser will enable precise control of pulse time and shape so that we can

[3] Longer pulses have reduced space charge effects and, thus, have higher electron dose that enable the acquisition of images with higher spatial resolution, e.g., with 1 μs electron pulse, image with sub-nanometer resolution can be acquired.

achieve better control of the drive conditions at the specimen, e.g., heating rate, isothermal holds, and cooling rate and thus providing a wide variety of temperature-time profiles at the sample. At present, the sample is rapidly heated with a pulse of ~10 ns duration (a number which we have very little ability to change), and it then cools according to its own thermal conductivity, usually on a time scale of 10-100 μs. By compensating the thermal conduction heat loss from the sample region of interest with an appropriately shaped pulse, we will be able to sustain the sample temperature at a constant level for some μs before allowing it to cool. This will enable a broad class of experiments in catalysis and surface science. The AWG capability also enables the production of electron pulse trains, an essential element of the planned DTEM “movie mode" of operation (discussed in next section). Multiple pulses with user set time delays between the pulses are also used for double exposure images to measure precise displacements of feature during dynamic events

4.2 Acquiring High-time Resolution Movies

The planned movie mode upgrade will enable multiple images or diffraction patterns to be acquired from a single sample drive event, thus producing a time history of a unique event. This capability will enable the study of phenomena that never unfold the same way twice, prime examples being defect motion in materials and irreversible nucleation and growth processes such as martensitic phase transformations. We plan to follow the approach developed at TU Berlin by Bostanjoglo [12], but with greater flexibility afforded by modern electronic and electron-optical technology.

The cathode laser AWG will be programmed to produce a series of electron pulses, each of which will capture a complete image or diffraction pattern. A fast multipole electrostatic deflector placed after the sample will deflect each image or diffraction pattern to its own region

on the camera. The camera will be read out at the end of the experiment and digitally segmented into a time- series of up to 16 images. The interframe times will on the order of ~100 ns or better, depending on the slew rate of the high voltage electronics. Future versions of movie mode may include fast-framing CCD technology, which can capture 100s of frames within a few μs. The main operating principle of these devices is that the photoelectron CCD data from multiple frames is stored in on-chip buffers that are readout at the end of the acquisition. Although these cameras are quite useful for optical measurements, the technology still needs development for use on electron microscopes, e.g., high-speed scintillators must be adapted to this technology and provide for detection of single 200 keV electrons.

5. Experimental Investigations on DTEM

5.1 Observing Transient Phenomena in Reactive Multilayer Foils

The high time resolution capabilities of the DTEM have been used to study the transient phases and morphological changes associated with rapid solid-state chemical reactions occurring in reactive multilayer foils (RMLF) [11, 14]. RMLFs, also called nanostructured metastable intermolecular composites, are layers of polycrystalline reactant materials that go through exothermic, self-propagating reactions when layer mixing is driven by an external stimulus [15-17]. Depending on composition, the number of bilayers and layer thicknesses, the exothermic reaction front can reach temperatures well above 1100 K and travel at a velocity of ~10m/s governed by interface diffusion [18-20]. Since RMLFs produce immense heat over a small surface area, they are used in applications as localized heat sources for material bonding or biological sterilization [15-17]. In addition, the periodic nano-construction makes RMLFs relevant for examination of *in situ* progression of interface-controlled diffusion and transient phase evolution.

Conventional methods lack the necessary combined spatial and time resolution to observe nanolayer mixing directly, leaving details of the reaction unclear. Using the time resolution in the DTEM, the transient states have now been observed *in situ*. Plan-view RMLFs are irreversibly reacted inside the DTEM by an infrared sample drive laser, then the transient states of the reaction front are observed with time-resolved diffraction and imaging. By studying the transient states of this dynamic material to understand the mechanisms that govern the rate of heat generation and transport, we can understand more about atomic diffusion between thin films and phase boundary motion for optimized engineering applications.

For these studies, we chose the Al/Ni-7wt%V multilayer system. The phase evolution and metastable phase formation were studied using 15 ns exposure, single-shot electron diffraction and brightfield imaging. The 15 ns "snap shot" diffraction data showing the phase evolution from discrete Al and NiV multilayers to the final intermetallic phase is illustrated in (Figure 5). The single-shot diffraction has been acquired in front of (t=0), in line with (t=300 ns), and beyond (t=∞) the reaction front region to detect the evolution of phase formation and metastable states. Thermal effects of the exothermic behavior in the material are evident by the diffuse background and reduction in higher order reflections in the time resolved 300ns diffraction pattern (Figure 5). When this hot NiAl structure cools to room temperature, concomitant grain growth processes preferentially texture the films, as indicted by the change in relative peak intensities. The primary conclusion in this study is that ordered B2 intermetallic NiAl phase forms within an extraordinarily short time period, <300 ns, which can expected due to short (few nm) atomic diffusion distances, high temperatures and high phase stability of the B2 structure at near equi-atomic compositions.

The reaction front appears as a sharp ring that moves outward, radially from the central laser initiation point, as shown in Figure 6a. The sharp transition between the unreacted and reacted material is consistent with the electron diffraction, indicating that the reactants form rapidly on the order of the 15 ns electron pulse. Closer examination of the microstructure (Figure 6b) revealed that the cellular structure forms directly behind the reaction front. Simple calculations of the heat released by the mixing of Al and Ni indicate that temperature rises on the order of 1700 K can be expected ($\Delta H \approx 77$ kJ mol^{-1} and $Cp^{Ni/Al}=24$ J mol^{-1} K^{-1}) [21]. At those temperatures and 60 at. % Ni, the material can be in a two phase state, solid-NiAl+liquid-NiAl. This may explain the dark contrast line, which may be related to the liquid structure, and a well-defined periodicity (~750 nm) that is analogous to cellular liquid-solid structures in alloy solidification [22]. These cellular microstructures only persist for 2-3μs after the reaction front passes and are not typically present in the post mortem microstructure, and although the mechanism for their formation is still not clear, their appearance gives reasonable estimates of the local temperatures reached at the reaction front, which is relevant, new data for modeling these systems.

5.2 Rapid First Order Transformations

The study of martensitic phase transformation is well suited for the capabilities of the DTEM. These transformations are defined as solid-solid structural transformations that are diffusionless and occur by nucleation and growth process. These types of transformation are lattice distortive and shear dominant, where the kinetics and final martensite microstructure are defined by the local strain energy. Since the transformation is diffusionless, atoms move in a coordinated manner to accomplish the structural transition where growth velocities can approach the 1/3 speed of sound [23]. Due to the innate speed of these interfaces, experimental

observation of the interface structure and even the overall transformations kinetics has been difficult. Hence, the high time resolution of the DTEM can be used to bring new insight into the interface dynamics and nucleation mechanisms in martensitic phase transformations.

For the first experiments, the high temperature phase transformation in Ti was studied. Titanium is a dimorphic element which undergoes a crystal structure change from HCP (α-phase) to the BCC (β-phase) atomic coordination upon heating above 1155K, which is accomplished by a simple shear strain of the HCP unit cell [24]. The fast kinetics of α to β phase transformation in nanocrystalline Ti films were investigated using single-shot electron diffraction and brightfield TEM images [25-28]. The selected area electron diffraction patterns (SAEDP) were taken at different delays between the heating, drive laser pulse and the electron pulse and with different drive laser energies. The laser induced temperature change was determined by correlating the observed onset of melting in the SAEDP with laser energy, which was then used as a one-point temperature calibration for subsequent experiments. The SAEDP were rotationally averaged to increase the signal to noise ratio, and the variation in radial intensity distribution as a function of scattering vector was plotted and compared to modeled intensities and distributions for the α-phase and β-phase, as shown in Figure 7.

Using Rietveld fitting routines [29], the phase fractions and corresponding α to β transformation rates were determined for temperatures between transition start (1155 K) and melt temperature (1943K). The experimental data were summarized in a time-temperature-transformation (TTT) curve with nanosecond time resolution (see Figure 8). Theoretical TTT curves were calculated using analytical models for isothermal martensite, available thermodynamic data, and experimental data gathered from pulsed electron brightfield TEM images. Above 1300K, there is excellent agreement between experiment and the discrete-

obstacle interaction model [30], suggesting that the nucleation rate and thermally assisted motion of the martensite interface are controlled by interface-solute atom interactions. However, theory predicts much slower transformation rates near the transition temperature than experiment. Experimental data fits using the Pati-Cohen model [31, 32] suggests that an increase in autocatalytic nucleation may partially account for the fast transformation rates at lower temperatures. It is also speculated that the transition temperature may be lower for the nanocrystalline material and may also explain the discrepancy.

Another important finding of this study was that incubation times for nucleation are strongly dependent on grain size, e.g. Ti foil with an average grain size of 40-75 nm have incubation times of ~100 ns, while materials with 100 μm grain sizes have incubation times on the order of 500 ns. This suggests that numerous grain boundaries in nanocrystalline materials act as strong defects and heterogeneous sites for nucleation, reducing the nucleation barrier energy and increasing transformation rate. A second observable difference between the nanocrystalline and coarse-grained Ti was in the repeatability of the transformation. After one laser shot, the microstructure of the nanocrystalline material changed dramatically, and after repeated shots to the same region, the film ceased to transform to the β-phase, indicating that the film may have adsorbed some oxygen, which is an α-phase stabilizer [23]. In coarse-grained materials, only one BCC variant was formed during the laser heating, and the microstructure reverted to the initial HCP crystal orientation and grain sizes upon cooling. The transformation characteristics were repeatable with continued shots to the same region with no observable change in incubation times or transformation rates. It is not completely understood why only one crystallographic variant (6 variants are possible) forms and why the transformation is crystallographically reversible. To clarify these issues, future experiments will use time-resolved

bright-field imaging to study the grain size dependence on nucleation processes (e.g. observe nucleation sites and autocatalytic processes) and martensite/parent interface dynamics.

5.3 Laser-assisted Nanowire Growth

One aspect of nucleation and growth that is being studied in detail in the DTEM relates to nanowire growth. In order to successfully produce nanoscale materials for applications such as optoelectronic devices and sensors [33-41], it is vital to have controlled fabrication of the one dimensional (1D) nanostructures. Limitations of current characterization techniques for the nucleation and growth mechanisms for 1D nanocrystalline materials do not allow for the understanding of and, thus, the ability to control the evolution of texture, morphology and crystal defects during processing.

The vapor-liquid-solid (VLS) process first described by Wagner and co-workers [42] is a widely accepted description for 1D nanostructure, or nanowire (NW) formation. The VLS describes growth as a two step process: (1) the first step involves the formation of liquid metal (catalyst) droplets that act as absorption sites for gas-phase reactants, (2) the supersaturated cluster then grows anisotropically into a NW with continued deposited of reactant vapor. This method has been proven to successfully produce crystalline NWs, however size control is limited to the catalyst metal droplet diameter [40]. Other approaches to NW growth are laser-based methods, such as hybrid pulsed-laser ablation/chemical vapor deposition (PLA/CVD) [40] and laser assisted NW growth at elevated temperatures [33, 34, 36, 38, 39], require the use of a pulsed laser to ablate a pellet target held at an elevated temperature in the presence of a reactive gas. Though proven to produce NWs, the number of variables involved in this experimental method yields a myriad of different morphologies [34, 39]. In light of the need for control during VLS growth of NWs, in-situ TEM-based growth methods have been used to study nucleation

and growth mechanisms [35, 37]. Studies of Si NW growth in the presence of oxygen have shown that the interface between liquid metal catalyst droplet and wire 'body' is a defining factor in controlled growth of NWs. These experiments were limited, however, by the 30Hz frame rate of video acquisition using conventional in-situ TEM. Using the high time resolution and *in situ* capabilities of the DTEM, we can treat an electron transparent target using a pulsed drive laser and monitor the stages of NW growth using nanosecond pulsed electron probe.

Films of <111> Si with a 4nm Au layer (as a catalyst) and Si/SiO_2 were treated with a frequency tripled (355nm) Nd:YAG laser with a 8 ns pulse rate inside the DTEM. No additional heat or gas was introduced in the TEM chamber, and thus, NW growth was controlled by a single variable: laser intensity. By controlling the laser energy, we can melt or ablate samples to raw materials needed to produce NW. Figures 9 A and B show images collected during the development of Au catalyzed Si wires by multiple pump laser shots and combined laser-melting and ablation of a 4nm Au coated Si substrate. Multiple NWs that protrude from the Si substrate were produced by ablation of a Si-SiO_2 sample with a single drive laser pulse, as shown in Figure 9C. The wires resembled those produced during laser assisted growth experiments by Morales and Lieber [36], yet NW production did not require gas flow or a steady-state temperature increase, unlike their experimental apparatus. In both cases, the NWs were produced by monitoring only laser energy for ablation or melting. Thus, the DTEM allows for controlled, in-situ, synthesis and characterization of NWs at nanosecond time scales. A complete understanding of the origin of texture, morphology and extended defects in NWs during nucleation and growth will allow for a more comprehensive model of the mechanisms involved in 1D nanostructure fabrication.

6. Conclusions

The high time resolution of *in situ* observations afforded by the unique capabilities of DTEM has brought new and fundamental insights into the phases and morphological evolution occurring in rapid chemical reactions of Ni-Al RMLFs, the nucleation behavior of α to β martensitic transformation in nanocrystalline Ti, and laser-assisted catalyzed growth of Si nanowires. Planned and ongoing improvements to the electron optics and laser systems will continue to expand the instrument's capabilities, which at present include the unique ability to capture single-shot images with 15 ns and 10 nm spatiotemporal resolution. The DTEM enables a new class *in situ* experiments that has orders higher time resolutions than standard techniques, and as the technology progresses, we expect many more exciting developments in the field.

Acknowledgements

We would like to acknowledge the fantastic technical assistance of Richard Shuttlesworth and Benjamin Pyke. Work was performed under the auspices of the U.S. Department of Energy by the University of California, Lawrence Livermore National Laboratory and supported by the Office of Science, Office of Basic Energy Sciences, Division of Materials Sciences and Engineering, of the U.S. Department of Energy under contract No. DE-AC52-07NA27344 with LLNL.

References

[1] P. E. Batson, N. Dellby, and O. L. Krivanek, "Sub-angstrom resolution using aberration corrected electron optics (vol 418, pg 617, 2002)," *Nature*, vol. 419, pp. 94-94, 2002.

[2] K. W. Urban, "The new paradigm of transmission microscopy," *Mrs Bulletin*, vol. 32, pp. 946-952, 2007.

[3] W. E. King, G. H. Campbell, A. Frank, B. Reed, J. F. Schmerge, B. J. Siwick, B. C. Stuart, and P. M. Weber, "Ultrafast electron microscopy in materials science, biology, and chemistry," *Journal of Applied Physics*, vol. 97, pp. 111101, 2005.

[4] W. E. King, M. Armstrong, V. Malka, B. W. Reed, and A. Rousse, "Ultrafast imaging of materials: Exploring the gap of space and time," *Mrs Bulletin*, vol. 31, pp. 614-619, 2006.

[5] B. J. Siwick, J. R. Dwyer, R. E. Jordan, and R. J. D. Miller, "Femtosecond electron diffraction studies of strongly driven structural phase transitions," *Chemical Physics*, vol. 299, pp. 285-305, 2004.

[6] K. Sokolowski-Tinten, C. Blome, C. Dietrich, A. Tarasevitch, M. H. von Hoegen, D. von der Linde, A. Cavalleri, J. Squier, and M. Kammler, "Femtosecond x-ray measurement of ultrafast melting and large acoustic transients," *Physical Review Letters*, vol. 8722, pp. art. no.-225701, 2001.

[7] D. J. Bradley, A. G. Roddie, W. Sibbett, M. H. Key, M. J. Lamb, C. L. S. Lewis, and P. Sachsenmaier, "Picosecond X-Ray Chronoscopy," *Optics Communications*, vol. 15, pp. 231-236, 1975.

[8] M. BenNun, J. S. Cao, and K. R. Wilson, "Ultrafast X-ray and electron diffraction: Theoretical considerations," *Journal of Physical Chemistry A*, vol. 101, pp. 8743-8761, 1997.

[9] T. LaGrange, M. R. Armstrong, K. Boyden, C. G. Brown, G. H. Campbell, J. D. Colvin, W. J. DeHope, A. M. Frank, D. J. Gibson, F. V. Hartemann, J. S. Kim, W. E. King, B. J. Pyke, B. W. Reed, M. D. Shirk, R. M. Shuttlesworth, B. C. Stuart, B. R. Torralva, and N. D. Browning, "Single-shot dynamic transmission electron microscopy," *Applied Physics Letters*, vol. 89, 2006.

[10] M. R. Armstrong, B. W. Reed, B. R. Torralva, and N. D. Browning, "Prospects for electron imaging with ultrafast time resolution," *Applied Physics Letters*, vol. 90, 2007.

[11] M. R. Armstrong, K. Boyden, N. D. Browning, G. H. Campbell, J. D. Colvin, W. J. DeHope, A. M. Frank, D. J. Gibson, F. Hartemann, J. S. Kim, W. E. King, T. B. LaGrange, B. J. Pyke, B. W. Reed, R. M. Shuttlesworth, B. C. Stuart, and B. R. Torralva, "Practical considerations for high spatial and temporal resolution dynamic transmission electron microscopy," *Ultramicroscopy*, vol. 107, pp. 356-367, 2007.

[12] H. Domer and O. Bostanjoglo, "High-speed transmission electron microscope," *Review of Scientific Instruments*, vol. 74, pp. 4369-4372, 2003.

[13] A. Rose, *Adv. Electron*, pp. 131, 1948.

[14] J. Kim, "Direct Imaging of Transient Structures using Nanosecond *in situ* TEM," Lawrence Livermore National Laboratory, 2008.

[15] J. Wang, E. Besnoin, O. M. Knio, and T. P. Weihs, "Effects of physical properties of components on reactive nanolayer joining," *Journal Of Applied Physics*, vol. 97, 2005.

[16] J. Wang, E. Besnoin, A. Duckham, S. J. Spey, M. E. Reiss, O. M. Knio, and T. P. Weihs, "Joining of stainless-steel specimens with nanostructured Al/Ni foils," *Journal Of Applied Physics*, vol. 95, pp. 248-256, 2004.

[17] A. J. Gavens, D. Van Heerden, A. B. Mann, M. E. Reiss, and T. P. Weihs, "Effect of intermixing on self-propagating exothermic reactions in Al/Ni nanolaminate foils," *Journal Of Applied Physics*, vol. 87, pp. 1255-1263, 2000.

[18] A. B. Mann, A. J. Gavens, M. E. Reiss, D. VanHeerden, G. Bao, and T. P. Weihs, "Modeling and characterizing the propagation velocity of exothermic reactions in multilayer foils," *Journal Of Applied Physics*, vol. 82, pp. 1178-1188, 1997.

[19] E. Besnoin, S. Cerutti, O. M. Knio, and T. P. Weihs, "Effect of reactant and product melting on self-propagating reactions in multilayer foils," *Journal Of Applied Physics*, vol. 92, pp. 5474-5481, 2002.

[20] C. Michaelsen, K. Barmak, and T. P. Weihs, "Investigating the thermodynamics and kinetics of thin film reactions by differential scanning calorimetry," *Journal Of Physics D-Applied Physics*, vol. 30, pp. 3167-3186, 1997.

[21] L. Perring, J. J. Kuntz, F. Bussy, and J. C. Gachon, "Heat capacity measurements on the equiatomic compounds in Ni-X (X = Al, In, Si, Ge and Bi) and M-Sb (with M = Ni, Co and Fe) systems," *Intermetallics*, vol. 7, pp. 1235-1239, 1999.

[22] D. A. Porter and K. E. Easterling, *Phase Transformations in Metals and Alloys*, Second edition ed. Delta Place, United Kingdom: Nelson Thrones Ltd., 1992.

[23] V. Raghaven, *Martensite: A Tribute to Morris Cohen*. Materials Park: AMS International, 1992.

[24] G. Lütjering and J. C. Williams, *Titanium*. New York: Springer-Verlag Berlin Heidelberg, 2003.

[25] T. LaGrange, G. H. Campbell, P. E. A. Turchi, and W. E. King, "Rapid phase transformation kinetics on a nanoscale: Studies of the α to β transformation in pure, nanocrystalline Ti using the nanosecond dynamic transmission electron microscope," *Acta Materialia*, vol. 55, pp. 5211-5224, 2007.

[26] T. LaGrange, G. H. Campbell, J. D. Colvin, B. Reed, and W. E. King, "Nanosecond time resolved electron diffraction studies of the alpha ->beta in pure Ti thin films using the dynamic transmission electron microscope (DTEM)," *Journal Of Materials Science*, vol. 41, pp. 4440-4444, 2006.

[27] G. H. Campbell, T. B. LaGrange, W. E. King, J. D. Colvin, A. Ziegler, N. D. Browning, H. Kleinschmidt, and O. Bostanjoglo, "The HCP to BCC phase transformation in Ti characterized by nanosecond electron microscopy," in *Solid-Solid Phase Transformations In Inorganic Material 2005, Vol 2*, 2005, pp. 443-448.

[28] H. Kleinschmidt, A. Ziegler, G. H. Campbell, J. D. Colvin, and O. Bostanjoglo, "Phase transformation analysis in titanium at nanosecond time resolution," *Journal of Applied Physics*, vol. 98, pp. -, 2005.

[29] H. M. Rietveld, "A Profile Refinement Method for Nuclear and Magnetic Structures," *Journal of Applied Crystallography*, vol. 2, pp. 65-&, 1969.

[30] M. Grujicic, G. B. Olson, and W. S. Owen, "Mobility of Martensitic Interfaces," *Metallurgical Transactions a-Physical Metallurgy and Materials Science*, vol. 16, pp. 1713-1722, 1985.

[31] S. R. Pati and M. Cohen, "Nucleation of Isothermal Martensitic Transformation," *Acta Metallurgica*, vol. 17, pp. 189-&, 1969.

[32] S. R. Pati and M. Cohen, "Kinetics of Isothermal Martensitic Transformations in an Iron-Nickel-Manganese Alloy," *Acta Metallurgica*, vol. 19, pp. 1327-&, 1971.

[33] X. F. Duan and C. M. Lieber, "Laser-assisted catalytic growth of single crystal GaN nanowires," *Journal Of The American Chemical Society*, vol. 122, pp. 188-189, 2000.

[34] J. L. Gole, J. D. Stout, W. L. Rauch, and Z. L. Wang, "Direct synthesis of silicon nanowires, silica nanospheres, and wire-like nanosphere agglomerates," *Applied Physics Letters*, vol. 76, pp. 2346-2348, 2000.

[35] S. Kodambaka, J. B. Hannon, R. M. Tromp, and F. M. Ross, "Control of Si nanowire growth by oxygen," *Nano Letters*, vol. 6, pp. 1292-1296, 2006.

[36] A. M. Morales and C. M. Lieber, "A laser ablation method for the synthesis of crystalline semiconductor nanowires," *Science*, vol. 279, pp. 208-211, 1998.

[37] E. A. Stach, P. J. Pauzauskie, T. Kuykendall, J. Goldberger, R. R. He, and P. D. Yang, "Watching GaN nanowires grow," *Nano Letters*, vol. 3, pp. 867-869, 2003.

[38] K. Wang, S. Y. Chung, and D. Kim, "Morphology of Si nanowires fabricated by laser ablation using gold catalysts," *Applied Physics A-Materials Science & Processing*, vol. 79, pp. 895-897, 2004.

[39] N. Wang, Y. H. Tang, Y. F. Zhang, C. S. Lee, and S. T. Lee, "Nucleation and growth of Si nanowires from silicon oxide," *Physical Review B*, vol. 58, pp. 16024-16026, 1998.

[40] Y. Wu, Y. Cui, L. Huynh, C. J. Barrelet, D. C. Bell, and C. M. Lieber, "Controlled growth and structures of molecular-scale silicon nanowires," *Nano Letters*, vol. 4, pp. 433-436, 2004.

[41] Y. Y. Wu, R. Fan, and P. D. Yang, "Block-by-block growth of single-crystalline Si/SiGe superlattice nanowires," *Nano Letters*, vol. 2, pp. 83-86, 2002.

[42] R. S. Wagner and W. C. Ellis, "Vapor-Liquid-Solid Mechanism Of Single Crystal Growth (New Method Growth Catalysis From Impurity Whisker Epitaxial + Large Crystals Si E)," *Applied Physics Letters*, vol. 4, pp. 89-&, 1964.

Figure Captions

Figure 1: General schematic of the LLNL. Notice that a section with a window and mirror has been inserted between the gun and condenser sections of the microscope to direct light from the cathode laser to the cathode.

Figure 2: Single-shot 15-nanosecond image of a Au/C grating showing resolution less than 10 nanometers.

Figure 3: Brightfield TEM images of 6061 Al sample containing secondary phase precipitates (a) conventional TEM image, (b) 15 ns exposure, single-shot pulsed image. Notice that at low magnification the single-shot pulsed and CW images are similar and exhibit the same information.

Figure 4: Schematic beam paths in the gun, accelerator, and condenser lenses for (a) conventional CW TEM, (b) the DTEM as described in the present report, and (c) the near-future DTEM with the added C0 lens. While the conventional design is an excellent optimization for few-second exposure times, many DTEM experiments call for a broader ability to sacrifice spatial coherence for increased signal without introducing excessive aberrations. The weak C0 lens solves this problem.

Figure 5: 15ns pulsed electron diffraction data acquired in front (t=0), in line with (t=300ns), and behind the reaction front (t=∞). The rotationally averaged distributions show that at t=300ns, an order B2 NiAl structure is formed that becomes highly textured when cooled to room temperature (t=∞).

Figure 6: 15ns exposure "snap-shot" images of the reaction front morphology, A) low magnification image the reacted zone (light contrast). Notice the sharp transition between unreacted (dark) and reacted (light), indicating the position of reaction front. B) higher magnification pulsed image of cellular microstructure which forms behind reaction front.

Figure 7: 15 ns exposure, single-shot electron diffraction data of the α to β transformation in nanocrystalline Ti occurring by laser induced temperatures of 1300K. Upper-right diffraction patterns show the transformation occurring from α-phase to β-phase at 1300 K and time delay of 1.5 μs, which after cooling back through the transition temperature transforms back to α-phase ($t=\infty$). Comparison of the rotationally averaged radial intensity distributions (plot on left-hand side) with simulated diffraction data (plot on lower right-hand side) indicate that transform to the β-phase was complete at 1.5 μs.

Figure 8: Experimental isothermal phase diagram for nanocrystalline Ti film constructed from quantitative analysis of the pulsed electron selected area diffraction data. Lines through are a smoothing curve fit through the data set [25].

Figure 9: A) Images of the development of a Si NW during laser-melting, showing the formation of a distinct catalyst bulb and wire. Images were taken after 12 laser pulses having 8 ns FWHM pulse duration B)a Si NW with a <111> growth direction, produced by laser ablation of a <111> Si substrate with 4nm of Au deposited on the surface to act as a catalyst. C) Clusters of Si NWs produced by single-shot laser ablation of a Si-SiO_2 film.

Figures

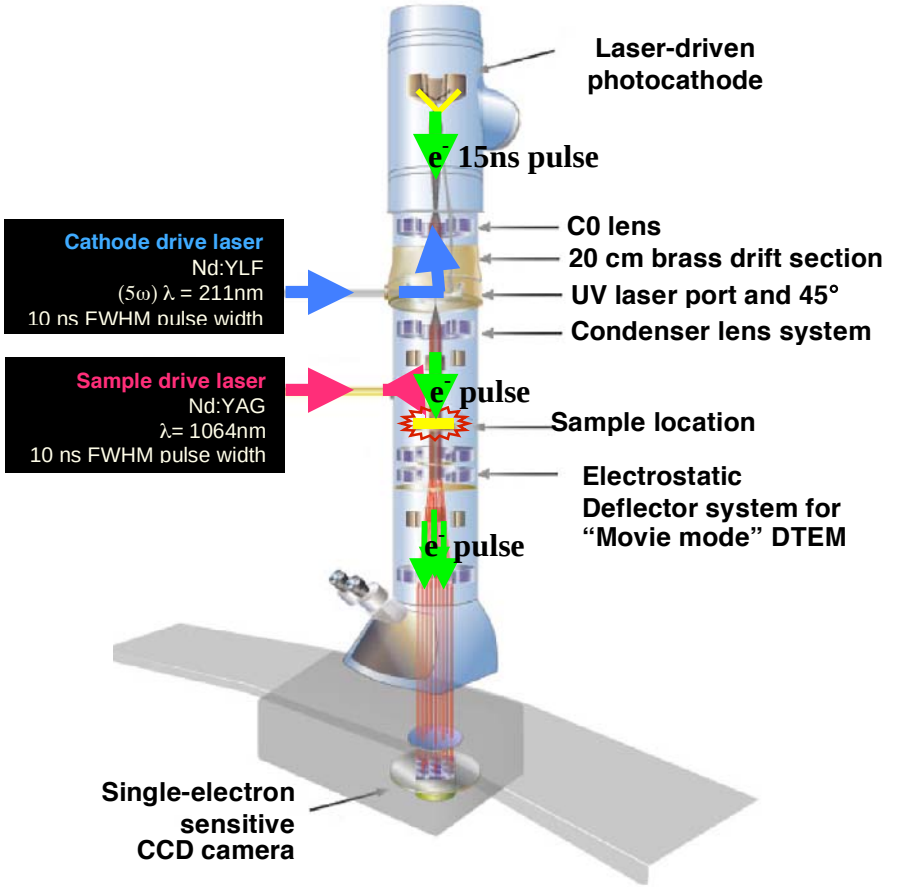

Figure 1

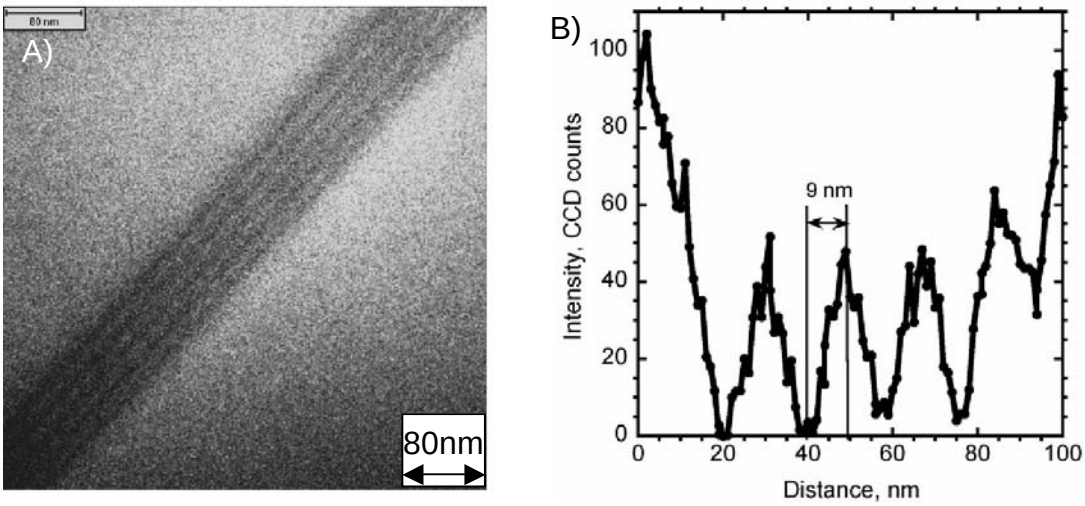

Figure 2

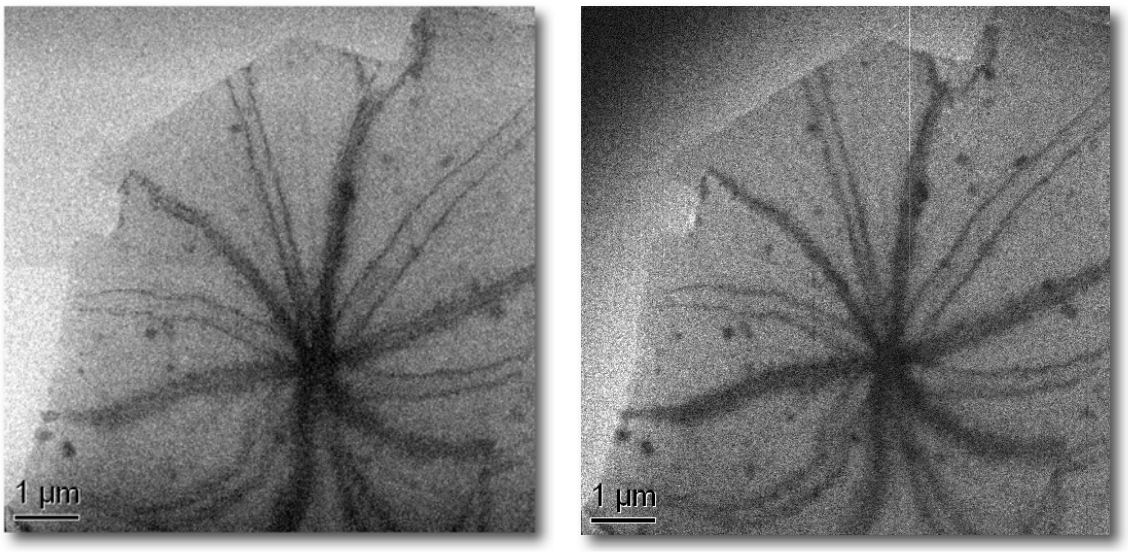

Figure 3

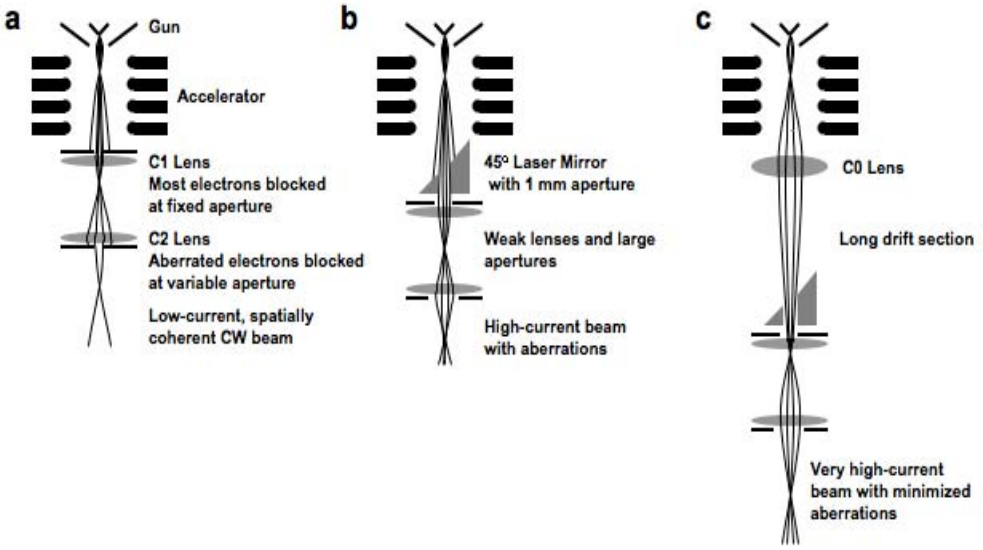

Figure 4

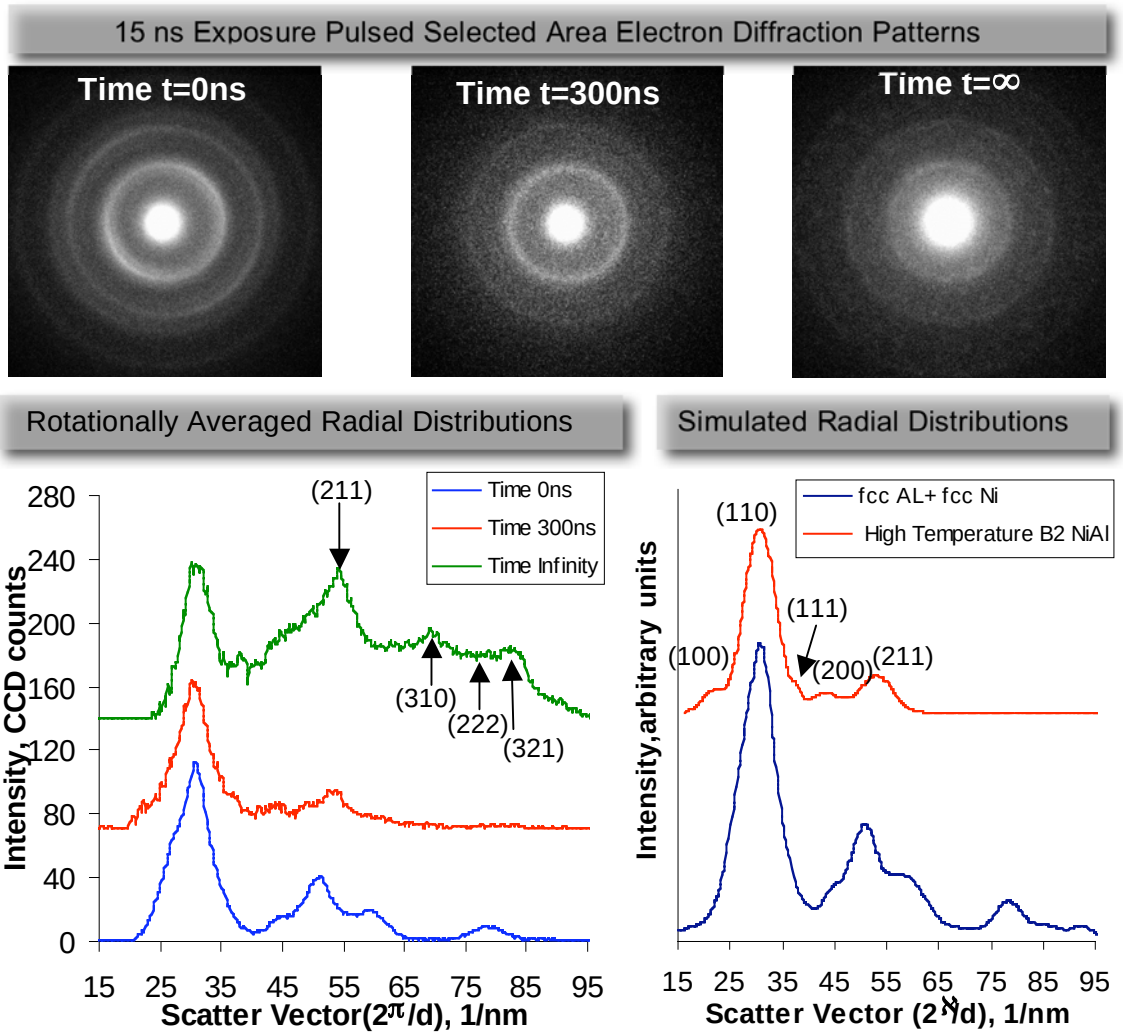

Figure 5.

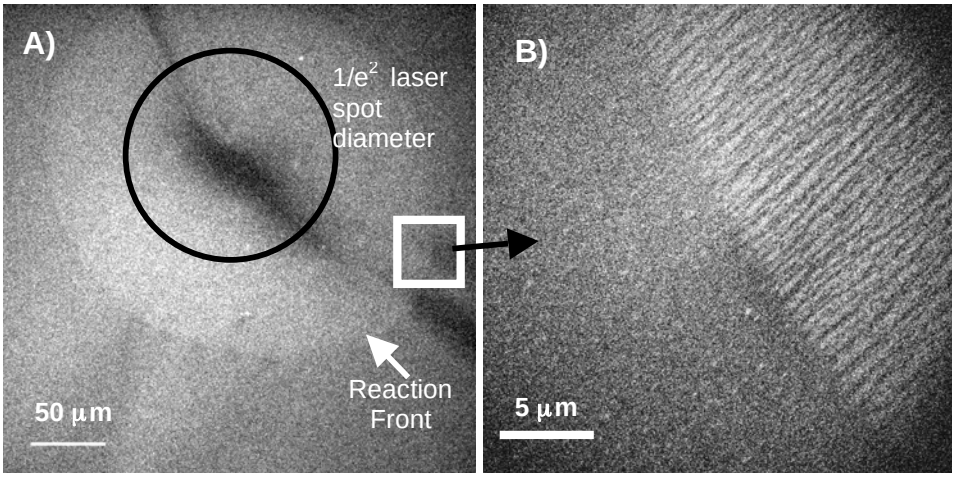

Figure 6.

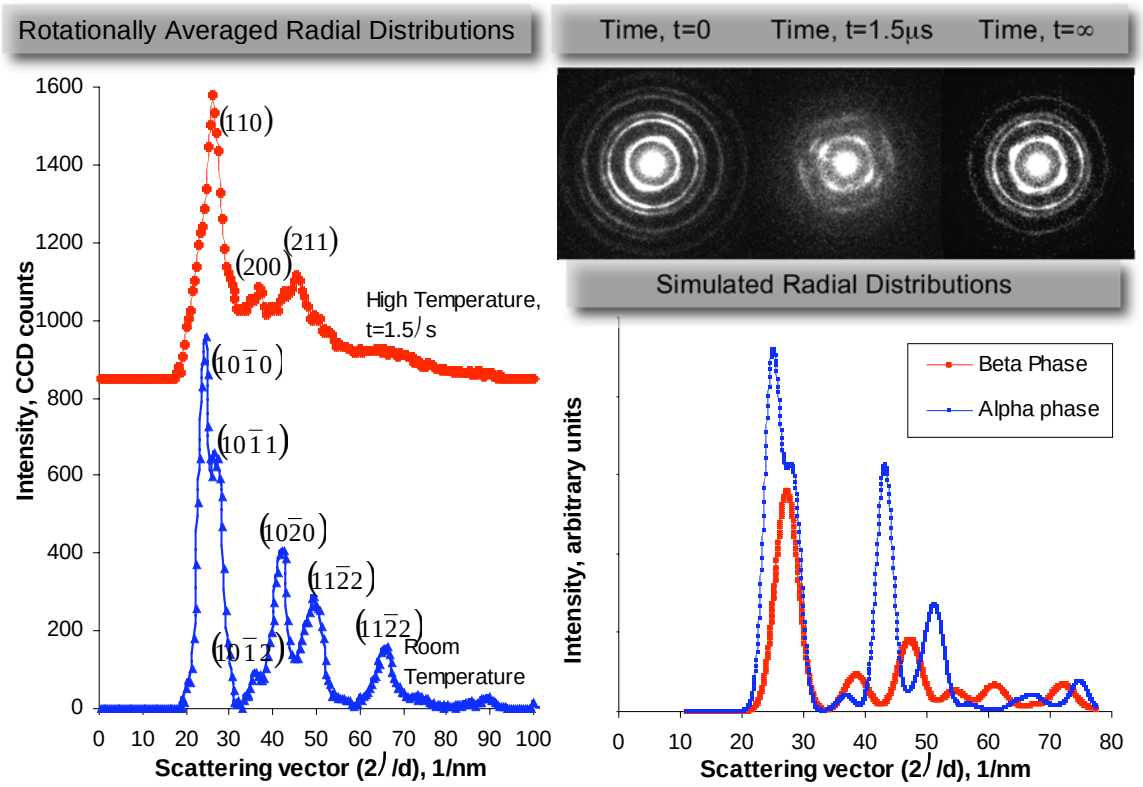

Figure 7.

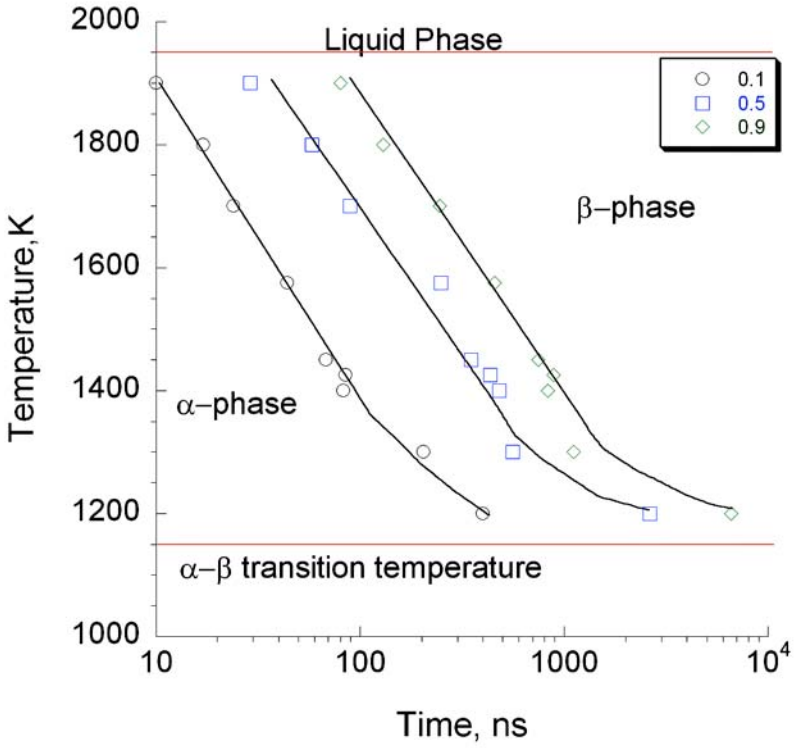

Figure 8.

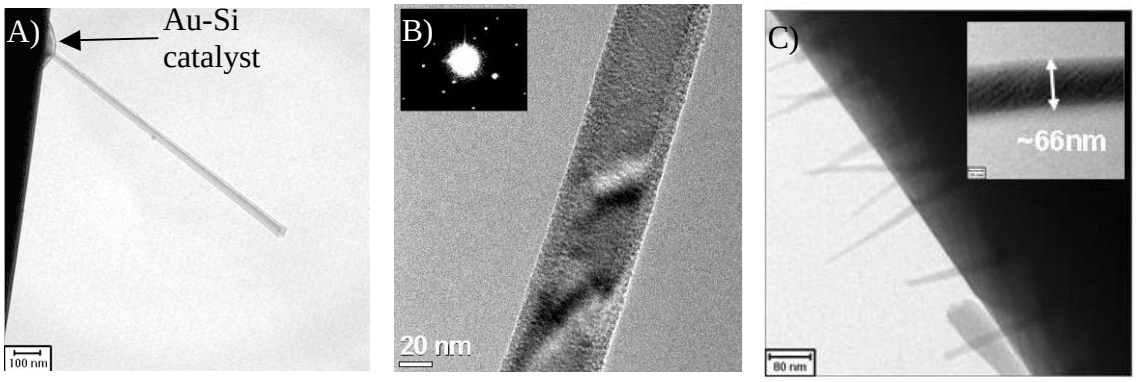

Figure 9.